Geosci. Model Dev. Discuss., 7, 6949–6996, 2014
www.geosci-model-dev-discuss.net/7/6949/2014/
doi:10.5194/gmdd-7-6949-2014

Geoscientific Model Development Discussions
Open Access

GNAQPMS-Hg v1.0, a global nested atmospheric mercury transport model: model description, evaluation and application to trans-boundary transport of Chinese anthropogenic emissions

H. S. Chen[1], Z. F. Wang[1], J. Li[1], X. Tang[1], B. Z. Ge[1], X. L. Wu[1], O. Wild[2], and G. R. Carmichael[3]

[1]LAPC, Institute of Atmospheric Physics, Chinese Academy of Sciences, Beijing, China
[2]Lancaster Environment Centre, Lancaster University, Lancaster, UK
[3]Center for Global and Regional Environmental Research (CGRER), University of Iowa, Iowa City, Iowa, USA

Received: 1 September 2014 – Accepted: 6 October 2014 – Published: 22 October 2014

Correspondence to: Z. F. Wang (zifawang@mail.iap.ac.cn)

Published by Copernicus Publications on behalf of the European Geosciences Union.

Abstract

Atmospheric mercury (Hg) is a toxic pollutant and can be transported over the whole globe due to its long lifetime in the atmosphere. For the purpose of assessing Hg hemispheric transport and better characterizing regional Hg pollution, a global nested atmospheric Hg transport model (GNAQPMS-Hg) has been developed. In GNAQPMS-Hg, the gas and aqueous phase Hg chemistry representing the transformation among three forms of Hg: elemental mercury (Hg(0)), divalent mercury (Hg(II)), and primary particulate mercury (Hg(P)) are calculated. A detailed description of the model, including mercury emissions, gas and aqueous phase chemistry, and dry and wet deposition is given in this study. Worldwide observations including extensive data in China have been collected for model evaluation. Comparison results show that the model reasonably simulates the global mercury budget and the spatial–temporal variation of surface mercury concentrations and deposition. Overall, model predictions of annual total gaseous mercury (TGM) and wet deposition agree with observations within a factor of two, and within a factor of five for oxidized mercury and dry deposition. The model performs significantly better in North America and Europe than in East Asia. This can probably be attributed to the large uncertainties in emission inventories, coarse model resolution and to the inconsistency between the simulation and observation periods in East Asia. Compared to the global simulation, the nested simulation shows improved skill at capturing the high spatial variability of Hg concentrations and deposition over East Asia. In particular, the root mean square error (RMSE) of simulated Hg wet deposition over East Asia is reduced by 24 % in the nested simulation. Model sensitivity studies indicate that Chinese primary anthropogenic emissions account for 30 and 62 % of surface mercury concentrations and deposition over China, respectively. Along the rim of the western Pacific, the contributions from Chinese sources are 11 and 15.2 % over the Korean Peninsula, 10.4 and 8.2 % over Southeast Asia, and 5.7 and 5.9 % over Japan. But for North America, Europe and West Asia, the contributions from China are all below 5 %.

GMDD

7, 6949–6996, 2014

1 Introduction

Since the Minamata Event in Japan in the 1960s (Harada, 1995), the toxicity of mercury (Hg) on human health and the environment has caused widespread public concern. Hg is a persistent, bio-accumulated pollutant, and the only heavy metal that can be transported globally in gaseous form (Schroeder and Munthe, 1998). As a result, Hg has been listed as a priority pollutant by many countries and international agencies. After a long struggle, the first global treaty (the Minamata Convention) aimed at reducing Hg emissions and releases, was adopted and signed by 92 countries in 2013 (http://www.unep.org/). This made an important advance towards joint action to control global Hg pollution and has brought higher requirements for understanding global Hg source–receptor relationships, especially the impacts of high regional emissions (e.g. from China and India) on global Hg levels. However, besides the remaining uncertainties in emission estimates, poor understanding of the chemical transformation of atmospheric mercury has made assessment of long-range transport very challenging (Pirrone and Keating, 2010).

Atmospheric mercury models are powerful tools to assess the fate and transport of mercury in the atmosphere. A number of atmospheric mercury models have been developed to investigate the emissions, transport, chemistry, deposition and source–receptor relationships of Hg at global and regional scales. Global models include the GEOS-Chem model (Selin et al., 2007), the CTM-Hg model (Seigneur et al., 2004), the CAM-Chem/Hg model (Lei et al., 2013), the ECHMERIT model (Jung et al., 2009), the MSCE-Hg-Hem model (Travnikov and Ilyin, 2009), the DEHM model (Christensen et al., 2004), and the GRAHM model (Dastoor and Davignon, 2009). Regional models include the CMAQ-Hg model (Bullock and Brehme, 2002), the STEM-Hg model (Pan et al., 2008), and the CAMx-Hg model (ENVIRON, 2011). Application of these models has greatly advanced our understanding of the global Hg cycle. However, several model intercomparison studies (Ryaboshapko et al., 2007; Bullock et al., 2008; Pirrone and Keating, 2010) have found that large uncertainties still exist in Hg models and there

GMDD
7, 6949–6996, 2014

is much room for improvement, especially for simulation of reactive gaseous mercury (RGM) and dry deposition.

Mercury is released to the atmosphere from both anthropogenic and natural sources. Human activities have increased the amount of mercury cycling through the atmosphere–ocean-terrestrial system by about a factor of three (Selin, 2009), although anthropogenic sources are estimated to account for only 31 % of total Hg emissions (Pirrone et al., 2010). China has the world's largest Hg production, consumption and emissions, and suffers the most serious Hg pollution (Jiang et al., 2006), but the impacts of its anthropogenic emissions on global Hg levels are still unclear. Previous modeling studies mainly focused on long-range transport of mercury from Asia. Based on the GEOS-Chem model, about 7–20 % of Hg deposition over the United States (US) was found to originate from Asian anthropogenic sources, which was comparable to that from North American sources (Strode et al., 2008; Jaffe and Strode, 2008). Another modeling study using the CTM-Hg model with three emission scenarios indicated that Asian anthropogenic emissions accounted for 14–25 % of Hg deposition over the US (Seigneur et al., 2004). Travnikov (2005) reported a contribution to Hg deposition from total Asian sources (including both anthropogenic and natural emissions) of 15 % over Europe and 33 % over the Artic. Corbitt et al. (2011) further pointed out that Asian emissions are the largest contributors to anthropogenic deposition to all ocean basins and these contributions are expected to further grow in the future. The above studies all treated Asian anthropogenic emissions as a whole, and the effects of anthropogenic emissions from the world's largest single emitter (China) have not been explicitly assessed before. In addition, due to lack of observational data, little model validation has been conducted over East Asia (especially China) in these studies and this leads to greater uncertainty in the conclusions. Fu et al. (2012) reviewed previous modeling studies and pointed out that current model simulations tend to underestimate total gaseous mercury (TGM) and total particulate mercury (TPM) concentrations but overestimate reactive gaseous mercury (RGM) concentrations in China. To improve Hg model skill in China, nested simulations with high horizontal resolution might be a good

GMDD
7, 6949–6996, 2014

choice. Zhang et al. (2012) demonstrated that a nested-grid model can capture the variation of Hg wet deposition over North America better than a global model.

Therefore, a comprehensive evaluation and improvement of Hg model performance in China is needed to effectively reduce the uncertainties in Hg trans-boundary transport and a quantitative assessment of Chinese anthropogenic contribution to global Hg concentration and deposition levels is helpful to determine and fulfill the Hg emission reduction tasks under the Minamata Convention.

In this paper, we describe the development of a global nested atmospheric mercury transport model (GNAQPMS-Hg) incorporating the latest available physical and chemical processes essential to the mercury life cycle. The spatial and temporal variability of Hg concentrations and deposition are comprehensively evaluated against available worldwide observations, including extensive data from China. The impact of horizontal resolution ($1^\circ \times 1^\circ$ in the global domain vs. $0.33^\circ \times 0.33^\circ$ in the nested domain) on model predictions over East Asia is examined. Finally, the trans-boundary transport of Chinese primary anthropogenic Hg emissions is quantified using the model.

2 Model description and setup

2.1 General description

The atmospheric physics and chemistry component of GNAQPMS-Hg, with the exception of the mercury module, is based on the Nested Air Quality Prediction Modeling System (NAQPMS) (Wang et al., 2006), developed at the Institute of Atmospheric Physics, Chinese Academy of Sciences. NAQPMS is a 3-D regional Eulerian model which has been rigorously evaluated and widely applied to simulate the chemical evolution and transport of ozone (Li et al., 2007; Tang et al., 2010), the distribution and evolution of aerosol and acid rain over East Asia (Wang et al., 2002; Li et al., 2011, 2012) and to provide operational air quality forecasts in mega cities such as Beijing, Shanghai and Guangzhou (Wang et al., 2009, 2010; Wu et al., 2012). GNAQPMS is

GMDD
7, 6949–6996, 2014

the global version of NAQPMS and uses the same model framework and physical and chemical parameterization schemes.

As a multi-scale model, GNAQPMS can simulate the transportation and formation of primary and secondary pollutants from urban to global scale using an online nesting approach. It includes advection, diffusion and convection processes, gas/aqueous/aerosol chemistry, and modules for dry and wet deposition. The advection process is parameterized based on an accurate mass conservative, peak-preserving algorithm provided by Walcek and Aleksic (1998). The gas phase chemical mechanism is the CBM-Z mechanism (Zaveri and Peters, 1999), including 133 reactions for 53 species. The dry deposition module uses the parameterization of Wesely (1989). The wet deposition and aqueous-phase chemistry module is constructed based on a revised version of the RADM mechanism (Chang et al., 1987; Wang et al., 2002; Ge et al., 2014). A mercury module has been developed and coupled into the GNAQPMS model in this study, as described in Sects. 2.2 to 2.4. Hereafter, we call this new model GNAQPMS-Hg. Note that meteorology, emissions, deposition and chemistry are self-consistent between the global and nested domains.

2.2 Mercury chemistry

In GNAQPMS-Hg, three forms of mercury are explicitly treated: elemental mercury (Hg(0)), divalent mercury (Hg(II)), and primary particulate mercury (Hg(P)). Transformations between these three forms include the gas phase oxidation of Hg(0) to Hg(II), the aqueous phase oxidation of Hg(0) to Hg(II), the aqueous phase reduction of Hg(II) to Hg(0), the aqueous phase equilibria of Hg(II) species and the aqueous phase adsorption of Hg(II) to PM. Figure 1 depicts the mercury reaction pathways both in the gas and aqueous phase while the detailed reactions and their rate constants are summarized in Table 1. In line with most global mercury models, GNAQPMS-Hg does not include bromine (Br) chemistry and dynamic air–surface exchange during Mercury Depletion Events (MDEs) in Polar regions (Schroeder et al., 1998) due to lack of fundamental data. Holmes et al. (2010) tested a Br oxidation mechanism in the GEOS-Chem

GMDD
7, 6949–6996, 2014

Hg model and found that including atomic Br as the sole Hg(0) oxidant produced TGM distributions consistent with most observations. However, Lei et al. (2013) demonstrated that adding Br chemistry has little impact on overall TGM patterns based on sensitivity experiments using the CAM-Chem Hg model and concluded that at the current level of understanding the O_3-OH oxidation mechanism alone is sufficient for Hg models.

In the gas phase, Hg(0) is oxidized to Hg(II) by O_3, OH, hydrogen peroxide (H_2O_2), hydrogen chloride (HCl) and molecular chlorine (Cl_2). The oxidized products of these five reactions are assumed to be in the gas phase. According to Lin et al. (2004), OH and O_3 are the dominant oxidants in the continental troposphere while Cl and Br dominate Hg(0) oxidation in the marine boundary layer and the upper troposphere. In the aqueous phase, Hg(0) is oxidized to Hg(II) by dissolved O_3, OH, and Cl_2, and Hg(II) can be reduced back to Hg(0) via reaction with HO_2 and by the formation of sulfite complexes. In addition, adsorption of Hg(II) species on atmospheric particulate matter (PM) is simulated using an adsorption coefficient ($K = 34\,\mathrm{L\,g^{-1}}$) recommended by Seigneur et al. (1998).

As shown in Table 1, the mercury chemistry requires the concentrations of several non-mercury species, among which O_3, OH, HO_2, H_2O_2, SO_2, HCl and PM are simulated online with GNAQPMS-Hg. However, Cl_2 is not explicitly simulated, and a typical vertical profile of Cl_2 concentrations is therefore prescribed. The Cl_2 concentrations are specified to be 100 ppt at the surface, 50 ppt aloft at night, 10 ppt during daytime over the oceans, and zero over land (Seigneur et al., 2001).

2.3 Mercury deposition

Deposition is the leading removal process of atmospheric mercury, and also a major cause of mercury contamination in soil and water. Studies have shown that both dry and wet removal pathways are equally significant for the total deposition of mercury (Pirrone and Keating, 2010; Lin et al., 2006).

GMDD
7, 6949–6996, 2014

Dry deposition of Hg(0), Hg(II) and Hg(P) is accounted for in the GNAQPMS-Hg model, and simulated with the Wesely (1989) resistance model, which considers the effect of different land cover types and characterizes the diurnal variation of dry deposition velocities. The Henry's Law constant for Hg(0) is set to be 0.11 M atm^{-1} (Lin and Pehkonen, 1999) with a temperature factor of −4970 K (Clever et al., 1985), and the surface reactivity is set to zero. Hg(II) represents $HgCl_2$ and $Hg(OH)_2$. Its Henry's Law constant is assumed to be the same as HNO_3 because they have similar solubility (Bullock and Brehme, 2002). Like HNO_3, Hg(II) has a strong tendency to stick to surfaces and its dry deposition occurs readily, so the surface resistance for Hg(II) in the dry deposition scheme is set to zero. The Hg(P) dry deposition velocity is set equal to that for sulfate, similar to that applied in the CMAQ-Hg and STEM-Hg model (Bullock and Brehme, 2002; Pan et al., 2008). Model intercomparison studies demonstrate that there are still very large uncertainties in Hg dry deposition estimates (Bullock et al., 2008), and this can be ascribed to the wide range of treatments and physical parameters for dry deposition used in different models.

The wet deposition of Hg includes in-cloud and below-cloud scavenging. In-cloud scavenging is dependent on cloud and rain water content, species solubility and chemical transformation in the liquid phase, while below-cloud scavenging depends mainly on total rainfall intensity and washout efficiency. Among the three forms of mercury, wet deposition of Hg(0) is minor compared to Hg(II) and Hg(P) due to its low solubility. Therefore, Hg(0) oxidation will enhance total Hg wet deposition. In the GNAQPMS-Hg model, wet deposition of Hg species is calculated through adapting the RADM mechanism. The physical properties (e.g. Henry's Law constant, surface reactivity, molecular diffusivity) used are the same as those in the dry deposition module. Currently, the uncertainties of Hg wet deposition simulation are mainly from the assumptions made in the cloud scavenging process and the uncertainty associated with the precipitation fields (Seigneur et al., 2001; Lin et al., 2006).

GMDD
7, 6949–6996, 2014

2.4 Mercury emissions

We include anthropogenic emissions, biomass burning emissions, geogenic emissions, land reemission and ocean emissions (including reemission) of Hg in the model. Emissions from artisanal mining and volcanoes are neglected due to lack of fundamental data. The former is estimated to be 400 Mg yr^{-1}, and the latter 90 Mg yr^{-1}, and they account for about 5 and 1 % of global total Hg emissions (Pirrone et al., 2010). Global Hg emissions in the model are compared to previous studies in Table 2, and their spatial distributions are given in Figs. S1–S3 in the Supplement.

Anthropogenic emissions in 2000 are derived from the Arctic Monitoring and Assessment Programme (AMAP) inventory (Pacyna et al., 2006; Wilson et al., 2006). This inventory has a horizontal resolution of 0.5° × 0.5° and no seasonal variation. Following Selin et al. (2008), we increase the Asian (0–60° N, 65–150° E) Hg(0) emissions in the AMAP inventory by 50 % (about 300 Mg yr^{-1}) to account for the regional underestimation identified by Jaffe et al. (2005). The modified inventory has a total emission of 2488 Mg yr^{-1}, with Hg(0), Hg(II) and Hg(P) accounting for 63, 29 and 8 % respectively. The major source regions are Asia and Africa, accounting for 59 % (1480 Mg yr^{-1}) and 16 % (399 Mg yr^{-1}), while Europe and North America contribute only 7 and 6 %. China has the largest emissions at country level (about 785 Mg yr^{-1}), contributing 53 and 32 % to the Asian and global anthropogenic Hg emissions, respectively.

Biomass burning emissions are specified by mapping an annual mean value of 675 Mg yr^{-1} (Friedli et al., 2009) to the spatial and temporal distribution of CO biomass burning emissions from the IPCC-AR5 (Intergovernmental Panel on Climate Change Fifth Assessment Report) emissions inventory (Lamarque et al., 2010). The regional and monthly emission amounts are prescribed based on Friedli et al. (2009). A similar method has been used by Jung et al. (2009).

The geogenic emissions here represent mobilization of Hg by degassing from geological reservoirs. Following Selin et al. (2007), we consider a geogenic source of

GMDD
7, 6949–6996, 2014

500 Mg yr^{-1} distributed according to the locations of Hg mines (Frank, 1999) as an indicator of Hg deposits. No temporal variation is applied to the geogenic emissions.

Land and ocean emissions are not dynamically calculated in the model due to the large uncertainties associated with current parameterizations. Consistent with several previous studies (Selin et al., 2007; Seigneur et al., 2001), the global annual land reemission of Hg is assumed to be 1500 Mg yr^{-1}. The biogenic CO emissions from the Global Emission InitiAtive (GEIA) inventory (Guenther et al., 2006) are used as spatial and temporal surrogates to map the land reemission. Regional emission totals from different latitude zones and land uses are prescribed based on Mason (2009).

Ocean emissions in our model are specified as 5000 Mg yr^{-1} (including reemission), close to the estimates of Selin et al. (2008). Similarly, ocean emissions are mapped according to the distribution of ocean biogenic CO emissions from the Precursors of Ozone and their Effects in the Troposphere (POET) inventory (Granier et al., 2005). Additionally, ocean emissions are adjusted to reflect several distribution characteristics: (1) ocean emissions are high in summer but low in winter (Strode et al., 2007), (2) ocean emissions are largest in the Tropics and downwind of industrial regions (Strode et al., 2007; Soerensen et al., 2010b), and (3) ocean emissions are large at mid and high latitudes in the Southern Hemisphere due to high wind speeds (Selin et al., 2008).

2.5 Model setup

Two nested domains covering the whole globe and East Asia are configured in this study. The horizontal resolutions are 1° × 1° and 0.33° × 0.33°, respectively. Vertically, the model uses 20 terrain-following layers from the surface to 20 km a.s.l., with a decreasing resolution with height. Roughly, the lowest 14–18 layers are in the troposphere and the remaining layers are in the stratosphere. The meteorological fields are provided by the global version of the Weather Research and Forecasting (WRF) model. The atmospheric lifetime of Hg(0) is 0.5–2 year (Schroeder and Munthe, 1998), and so to ensure mixing through the global troposphere and approach steady-state, we conduct

GMDD
7, 6949–6996, 2014

the simulation for a 4 year period, with the first 3 years used for initialization and the last year (2001) used for analyses.

Emissions of reactive gases and aerosols used in this study are from several databases: (1) the IPCC-AR5 anthropogenic and biomass burning emissions for 2000 (Lamarque et al., 2010), (2) the GEIA biogenic emissions for 2000 (Guenther et al., 2006) and lightning emissions of nitric oxide (NO_x) for 1983–1990 (Price et al., 1997), (3) the POET ocean emissions of volatile organic compounds (VOCs) for 2000 (Granier et al., 2005), (4) the soil NO_x emissions for 2001 from Yan et al. (2005). All emissions are interpolated and remapped to match the model grids of the global and nested domains.

The initial and top boundary conditions for O_3, NO_x, and CO are taken from a global chemical transport model (MOZART-V2.4) with 2.8° resolution (Horowitz et al., 2003). Initial surface concentrations for Hg(0) of 1.6 ng m^{-3} in the Northern Hemisphere and 1.2 ng m^{-3} in the Southern Hemisphere are prescribed and these decrease gradually with elevation (Lindberg et al., 2007).

Two model simulations, with and without Chinese primary anthropogenic Hg emissions, are carried out in this study. The differences between the two simulations are attributed to the influence of Chinese primary anthropogenic Hg emissions.

3 Model evaluation

3.1 Observational data

Compared to reactive gases and aerosols, atmospheric Hg measurements are still quite sparse. Routine monitoring networks for atmospheric Hg concentrations and deposition have only been established in Europe and North America. Lack of Hg observational data is a great restriction against advancing our understanding of global Hg cycling and improving our skill in modeling. There is an urgent need to establish a

GMDD
7, 6949–6996, 2014

coordinated global Hg monitoring network for current Hg study (Sprovieri et al., 2010; Keeler et al., 2009).

The observational dataset in this study is based partly on the database shared by the GEOS-Chem Hg modeling group (public access at https://github.com/noelleselin/HgBenchmark; Selin et al., 2007, 2008; Holmes et al., 2010). This is supplemented with scattered Hg observations across East Asia collected from the literature. The observations used in this study are summarized as follows: (1) long-term TGM/GEM (gaseous elemental mercury) measurements at 51 land sites, with 49 in the Northern Hemisphere and 2 in the Southern Hemisphere, (2) long-term RGM/TPM measurements at 26 land sites, all in the Northern Hemisphere, (3) short-term Hg species measurements from 6 ship cruises, (4) wet deposition measurements from the MDN (the Mercury Deposition Network in North America, http://nadp.sws.uiuc.edu/nadpdata/mdnalldata.asp) and EMEP (the European Monitoring and Evaluation Programme, http://www.nilu.no/projects/ccc/emepdata.html) monitoring networks, with 51 and 8 sites respectively, (5) dry and wet deposition measurements at 19 sites in East Asia. Further information about the measurement sites and data sources is given in Tables S1–S4 in the Supplement. It should be noted that the time periods of the measurements do not all match with those of the simulation, and this difference may partially explain any model–observation discrepancies.

3.2 Global mercury budget

Figure 2 gives the global mercury budget in GNAQPMS-Hg, including the cycling among atmosphere, ocean and land. The total atmospheric burden of Hg is 8679 Mg, with Hg(0), Hg(II), and Hg(P) contributing 92, 7 and 1 %, respectively. Therefore, mercury in the atmosphere exists mainly as Hg(0). Total emissions and deposition of Hg are 5163 and 2866 Mg yr^{-1} over land (a net source), and are 5000 and 7297 Mg yr^{-1} over ocean (a net sink), indicating that Hg is transported from land to ocean. For total deposition of Hg species, Hg(0) and Hg(II)/Hg(P) account for 38 and 62 % over the earth's surface. Over land, deposition of Hg(II)/Hg(P) is more prominent than that of

GMDD
7, 6949–6996, 2014

Hg(0), while they are both important over the ocean. Our results for total Hg deposition over ocean and Hg(II)/Hg(P) deposition over land are very close to that of GEOS-Chem (Selin et al., 2008). However, Hg(0) deposition over land derived from GNAQPMS-Hg is much smaller. This may be due to the lower reactivity coefficient used in the dry deposition module in GNAQPMS-Hg (zero in GNAQPMS-Hg but 10^{-5} in GEOS-Chem), which produces a lower dry deposition velocity for Hg(0).

Table 2 compares the GNAQPMS-Hg TGM budget and lifetime to those from previous modeling studies. The TGM sources, sinks, burden and lifetime estimated from GNAQPMS-Hg are all in the range determined by previous studies. Taking the TGM lifetime as an example, the reported range is 1.1 ± 0.4 years and it is 0.85 years for GNAPQMS-Hg. In addition, similar to the results of GEOS-Chem (Selin et al., 2007), Hg dry deposition in GNAQPMS-Hg dominates globally over wet deposition. Dry and wet deposition account for 78 and 22 %, respectively.

3.3 Total gaseous mercury (TGM)

As shown in Fig. 3, the main characteristics of the spatial distribution of TGM are captured well by the model. High surface TGM concentrations are found in or downwind of areas with intensive mercury-relative mining (e.g. Western USA, Southern Africa) and rapid industrialization (e.g. East Asia). In particular, TGM concentrations even exceed $3\,\mathrm{ng\,m^{-3}}$ in eastern China. Both model simulation and observations show a significant surface interhemispheric gradient in TGM (Figs. 3 and 4). Based on background observations, Lindberg et al. (2007) reported that mean Hg(0) concentrations were 1.5–1.7 $\mathrm{ng\,m^{-3}}$ in the Northern Hemisphere and 1.1–1.7 $\mathrm{ng\,m^{-3}}$ in the Southern Hemisphere. Lamborg et al. (2002) also estimated the range of north–south interhemispheric TGM concentration ratios for surface air as 1.2–1.8. Our model results share a general similarity with these studies. In GNAQPMS-Hg, surface mean TGM concentrations in the Northern and Southern Hemisphere are 1.56 and 1.23 $\mathrm{ng\,m^{-3}}$, and the derived interhemispheric ratio is 1.27. However, it should be noted that GNAQPMS-Hg is systematically biased low relative to cruise observations in the Northern Hemisphere,

GMDD
7, 6949–6996, 2014

which leads to underestimation of the TGM interhemispheric ratio compared with the range (1.49 ± 0.12) reported by Temme et al. (2003) based on observations from several Atlantic cruises. This disagreement was also found by several previous modeling studies (Seigneur et al., 2004; Selin et al., 2007), and can be attribute to the inability of current models to reproduce the air–sea exchange of Hg reasonably (Soerensen et al., 2010a). In general, the simulated TGM concentrations match observations within a factor of two (Fig. 10). The correlation coefficient (R) and normalized mean bias (NMB) between model results and observations from 51 land sites are 0.7 and −18 %, respectively (Table 3).

Figure 5 illustrates the mean seasonal variations of TGM concentrations in North America, Europe, East Asia, the Arctic, the Antarctic (Neumayer) and South Africa (Cape Point). In northern mid-latitudes, TGM concentrations are high in winter but low in summer. This seasonality can be reproduced well by GNAQPMS-Hg. The summer low is caused by high OH concentrations and frequent precipitation (Bergan and Rodhe, 2001). Compared with observations, the simulated TGM monthly variations are stronger in North America but weaker in East Asia. At Arctic and Antarctic sites, TGM shows a spring minimum driven by MDEs and a summer maximum driven by reemission from the snowpack (Steffen et al., 2005). The summer maximum is captured by GNAQPMS-Hg because high reemission in polar summer has been taken into account in our land reemission inventories. However, due to missing halogen chemistry, the model fails to reproduce the spring minimum. At Cape Point, both observed and simulated TGM show little seasonal variation. However, simulated monthly TGM concentrations are systematically biased high (NMB is 87 %), which can be attributed to an overestimation in AMAP emission inventories in South Africa (Lei et al., 2013).

3.4 Oxidized mercury

Figure 3 also shows the global distribution of oxidized mercury (defined as the sum of RGM+TPM in the observations and Hg(II)+Hg(P) in the model). Similar to TGM, a pronounced north–south interhemispheric gradient is found for surface concentrations of

GMDD
7, 6949–6996, 2014

oxidized mercury, which is consistent with the global distribution of emissions. Both model simulation and observations indicate that oxidized mercury concentrations are much higher in East Asia than North America and Europe. Compared to scarce available observations, oxidized mercury concentrations are overestimated by GNAQPMS-Hg in most parts of the world (except East Asia). This discrepancy may partially be attributed to excessive oxidation of Hg(0) by relatively high concentrations of OH and O_3 (especially over the ocean) and uncertainties concerning Hg chemical speciation in emission inventories. The simulated tropospheric mean OH concentration is 1.41×10^6 molec cm^{-3}. This is at the high end of the concentration range (0.65–1.56×10^6 molec cm^{-3}) summarized by Lawrence et al. (2001) and is about 27 % higher than the ensemble mean ($11.1 \pm 1.8 \times 10^5$ molec cm^{-3}) of the Atmospheric Chemistry and Climate Model Intercomparison Project (ACCMIP) models (Voulgarakis et al., 2013). The simulated mean surface O_3 in the North Pacific and North Atlantic is overestimated by 27 and 34 % compared to observations from the WDCGG (World Data Centre for Greenhouse Gases) network, although concentrations over land are reproduced relatively well (see Figs. S4–S5 in the Supplement). Overall, the simulated oxidized mercury concentrations agree with observations within a factor of five (Fig. 10). The statistical indicators, *R* and NMB, calculated from 26 land sites are 0.53 and 3 % (Table 3), respectively.

3.5 Wet deposition

Wet deposition is mainly determined by the distribution of precipitation and Hg concentrations. Figures 6 and 7 evaluate the simulated annual Hg wet deposition and accumulated precipitation over North America, Europe and East Asia. In general, GNAQPMS-Hg reproduces the spatial patterns of Hg wet deposition relatively well.

Over North America, the maximum wet deposition occurs in the southeast, corresponding to high OH concentrations and frequent precipitation there, while less wet deposition occurs in the west and north, where there is much less precipitation. GNAQPMS-Hg predicts the magnitude of mean wet deposition within 5 % and shows

GMDD
7, 6949–6996, 2014

a good spatial correlation ($R = 0.76$) (Table 3). These results are similar to those of GEOS-Chem (Selin et al., 2007). However, it should be also noted that precipitation in the southeast is slightly overestimated by the model.

Over Europe, model performance for wet deposition and precipitation are better than over North America and East Asia. High spatial correlation between the simulated and observed results are found for both wet deposition ($R = 0.78$) and precipitation ($R = 0.86$), and the NMBs are both less than 5 % (Table 3).

Over East Asia, Hg wet deposition is not only related to the precipitation pattern but also the local Hg emissions, especially in the southwest and Jilin province of China, and in Central Japan. Model performance for wet deposition over East Asia is poorer than over Europe and North America. Although the spatial distribution and magnitude of precipitation over East Asia are seemingly well reproduced ($R = 0.64$ and NMB = −6 %), a large underestimation (NMB = −61 %) of wet deposition is found here. Specifically, this is because the model fails to capture the high wet deposition at certain sites. For example, the observed wet deposition over Shanghai and Changchun are 251 and 108 $\mu g\,m^{-2}$ while the corresponding simulated values are only 25 and 13 $\mu g\,m^{-2}$. This suggests that it is hard for models with coarse horizontal resolution to characterize the high local mercury pollution in China. The difference between the simulated and observed time periods and uncertainties in the emission inventories may also contribute to these discrepancies.

Figure 8 further compares the simulated seasonal cycle of wet deposition with measurements at MDN sites over North America and EMEP sites over Europe. No monthly wet deposition observations are available over East Asia. Wet deposition and precipitation share similar monthly variations, with high values in summer and autumn and low values in winter, as shown by both observations and simulation. In summer and autumn, the variation in wet deposition and precipitation among sites is larger than for other seasons, and this is evident from the greater variability in Fig. 8. GNAQPMS-Hg tends to overestimate wet deposition and precipitation in July and August over North America.

GMDD
7, 6949–6996, 2014

3.6 Dry deposition

Due to limited observations, only Hg dry deposition over East Asia is evaluated in this study. Associated with local Hg emissions, high dry deposition mainly occurs over central eastern China and central Japan (Fig. 9). The modeled dry deposition has a good spatial correlation with observations (R = 0.81), but there is a substantial negative bias (NMB = −42 %, Table 3). In general, the simulated dry deposition agrees with observations within a factor of five (Fig. 10). Over Japan, the model results are biased high by a factor of 2–5, which may be caused by overestimation of Hg(II) and Hg(P) emissions. Taking Tokyo as an example, observed Hg(P) is only 98 pg m^{-3} while the simulated value is as high as 648 pg m^{-3}. Modeling studies conducted by Pan et al. (2008) using the STEM-Hg model also found large overestimation in dry deposition over Japan. Conversely, the model results are biased low by a factor of 2–5 over China, which indicates probable underestimation of Chinese Hg emissions.

3.7 Model performance summary and comparison

In this section, we summarize the statistical performance of GNAQPMS-Hg for TGM, oxidized mercury, and wet and dry deposition, compare the model performance over East Asia, North America and Europe, and assess the effects of horizontal resolution on model predictions over East Asia. As shown in Fig. 10, the simulated TGM and wet deposition are within a factor of two of the corresponding observations and within a factor of five for oxidized mercury and dry deposition. The statistical performance of GNAQPMS-Hg is comparable with that of other state-of-the-art Hg models (Bullock et al., 2008; Ryaboshapko et al., 2007; Pirrone and Keating, 2010).

3.7.1 East Asia vs. North America and Europe

As illustrated in Table 3, the model statistical performance for all Hg parameters in North America and Europe is better than in East Asia. For example, the RMSEs

GMDD
7, 6949–6996, 2014

between simulated and observed TGM over North America and Europe are 0.58 and 0.17 ng m^{-3} but up to 3.61 ng m^{-3} over East Asia. The poor model performance over East Asia is probably caused by the following reasons. Firstly, there are differences between simulated and observed data periods. Hg measurements over East Asia (especially China) are mainly taken from recent years, and the observed values are higher than in year 2001, which may lead to model underestimation. Secondly, there is a much higher spatial variation ratio (SVR, see Table 3) for Hg parameters in East Asia than North America and Europe. This implies that there are very intense spatial variations in Hg concentrations and deposition over East Asia which cannot be resolved at the coarse horizontal resolution used in global models. Thirdly, there are large uncertainties in emission inventories over East Asia. Large underestimations in Hg anthropogenic emissions over East Asia have been demonstrated in several previous studies (Jaffe et al., 2005; Pan et al., 2007; Friedli et al., 2004). This is consistent with the simulated results in this study.

3.7.2 Global vs. nested simulations

In order to assess the impact of resolution on model predictions, an online nested simulation with higher resolution (0.33° × 0.33°) over East Asia was conducted and compared to the global simulation with lower resolution (1° × 1°). Emissions, meteorology, deposition and chemistry are self-consistent between the global and nested domains. The nested simulation uses higher resolution model inputs (e.g. topography, meteorology, emissions) and thus has the potential to better resolve high spatial variability of Hg concentrations and deposition in regional and local scales.

Figures 7 and 9 compare the spatial distributions of simulated annual mercury wet deposition, accumulated precipitation and dry deposition over East Asia between the global and nested simulations. Although the global and nested simulations predict similar large scale patterns for Hg deposition, the nested simulation resolves many fine features which are lost in the global simulation by horizontal averaging. Firstly, in the nested domain, high deposition fluxes become more concentrated in regions with large

GMDD
7, 6949–6996, 2014

emissions or precipitation resulting in higher spatial variability in deposition. Secondly, the nested simulation reveals elevated wet deposition in southwest China due to frequent orographic and convective precipitation. Finally, the nested simulation shows a more detailed land/ocean contrast in deposition over coastal regions. For example, over the coastal regions of southeast China and Japan, wet deposition increases due to scavenging of local emissions and enhanced precipitation (Fig. 7) while dry deposition decreases associated with the lower dry deposition velocity of Hg(0) over land than over ocean (Fig. 9). Our results are similar to those of Zhang et al. (2012) who conducted a nested simulation of Hg over North America using the GEOS-Chem model.

Figure 11 and Table 3 further quantitatively compare the model performance over East Asia between the global and nested domains. In the Taylor diagram (Taylor, 2001), the position of each circle (or square) quantifies how closely the simulated results match observations. We can see that the simulated precipitation, oxidized Hg, wet and dry deposition agree better with observations in the nested domain than in the global domain (Fig. 11). The largest improvement is found in the simulated wet deposition. Specifically, the statistical parameter R for simulated wet deposition increases from 0.36 to 0.78, the NMB decreases from −61 to −28 %, and the RMSE decreases by 24 % (from 60.1 to 45.5 $\mu g\,m^{-2}\,yr^{-1}$) (Table 3). But for TGM, oxidized Hg and dry deposition, the statistical parameters do not change significantly. For example, the RMSEs of simulated oxidized Hg and dry deposition decrease by 7 and 2 % respectively, but increase by 7 % for simulated TGM.

4 Impacts of Chinese primary anthropogenic sources on global Hg levels

Figure 12 shows the contribution of Chinese primary anthropogenic sources (not including reemission) to annual mercury surface concentrations and total deposition in the Northern Hemisphere, and Fig. 13 gives the corresponding mean percentage contributions over different world regions (defined in Fig. S6 in the Supplement), as derived from a sensitivity simulation with Chinese anthropogenic emissions shut off. In general,

GMDD
7, 6949–6996, 2014

the largest percentage contribution is found in China itself, followed by neighbouring regions like the Korean Peninsula, Southeast Asia, Mongolia and Japan, but they are relatively small in other regions. Specifically, domestic anthropogenic emissions contribute on average 0.6 ng m^{-3} (ranging from below 0.1 to above 3.0) to surface Hg concentrations and 18.4 µg m^{-2} (ranging from below 2.0 to above 50.0) to total deposition in China. They account for about 30 and 62 % on a national basis, respectively. The domestic contribution to deposition consists mainly of the deposition of directly emitted Hg(II) and Hg(P) near sources and deposition of Hg(II) formed by oxidation of Chinese Hg(0). For neighboring regions, the Chinese anthropogenic contributions to Hg concentrations and deposition are also large. For example, the percentage contributions are 11 % (0.2–0.6 ng m^{-3}) and 15.2 % (8–20 µg m^{-2}) over the Korean Peninsula, 10.4 % (0.1–0.6 ng m^{-3}) and 8.2 % (1–12 µg m^{-2}) over Southeast Asia, and 5.7 % (0.1–0.4 ng m^{-3}) and 5.9 % (2–15 µg m^{-2}) over Japan. For regions far away from China, the percentage contributions are small. They are 4.2 % (0.06–0.1 ng m^{-3}) and 4.8 % (0.5–4 µg m^{-2}) over North America, and 3.5 % (below 0.08 ng m^{-3}) and 3.0 % (below 2.0 µg m^{-2}) over Europe. The percentage contributions over North America determined from our simulation are comparable with the modeling study of Lei et al. (2013). They estimated that around 7 % of TGM concentrations and 9 % of total Hg deposition in the United States resulted from transpacific transport of Asian anthropogenic emissions. Given that about 53 % of Asian anthropogenic Hg emissions are from China, it is reasonable that our estimated contributions are a little smaller than those reported by Lei et al. (2013).

Finally, there are another two issues which need to be addressed. Firstly, the above analysis mainly focuses on regional average contributions. However, the percentage contributions vary geographically inside the region. As shown in Fig. 12, contributions of domestic anthropogenic emissions to total deposition in Central Eastern China can exceed 40 µg m^{-2}, but they are below 5 µg m^{-2} in Western China. Similarly, previous studies have found that Asia emissions make a much larger contribution to Hg deposition in the Western USA than in the Eastern USA (Seigneur et al., 2004; Strode

GMDD
7, 6949–6996, 2014

et al., 2008). Secondly, the contributions from reemission of previously deposited anthropogenic Hg (treated as natural land or ocean reemission in GNAQPMS-Hg) are not taken into account in this study. Of the natural emissions, only one-third is considered not to be influenced by anthropogenic activities at all (Jung et al., 2009). In addition, according to the modeling study of Selin et al. (2008), 31 % (including 22 % primary and 9 % recycled) of the deposition over USA is from anthropogenic emissions outside of North America. When considering reemission of previously deposited anthropogenic Hg, this suggests that the foreign anthropogenic contribution would increase by about 42 % (from 22 to 31 %). If we apply the same scaling factor to our attribution results, then the estimated Chinese anthropogenic contributions to Hg deposition over North America would increase from 4.8 to 6.8 %. Therefore, it is also important to consider the reemission of previously deposited anthropogenic Hg.

5 Conclusions

A global nested atmospheric mercury transport model including Hg emissions, chemical transformation and deposition is introduced in this study. The treatment of Hg chemistry employs the O_3–OH oxidation and SO_3^{2-}–HO_2 reduction mechanisms. The gas phase reactions of Hg are added to the CBM-Z mechanism, while the aqueous phase reactions and wet deposition of Hg are calculated through adapting the RADM mechanism. The Wesely (1989) resistance model is used to deal with Hg dry deposition. The same meteorological fields, emissions, chemical and physical parameterizations are used in the global and nested domains.

The GNAQPMS-Hg model has a global mercury source of 10 163 Mg yr^{-1}, including 2488 Mg yr^{-1} primary anthropogenic emissions, 675 Mg yr^{-1} biomass burning emissions, 2000 Mg yr^{-1} land emissions (of which 75 % is reemission), and 5000 Mg yr^{-1} from the ocean. Dynamic bidirectional air–surface exchange of Hg is not included in the model. Instead, we simply apply static net emission fluxes to account for natural

GMDD
7, 6949–6996, 2014

sources (including reemission) of Hg, with total emission amounts determined based on published estimates.

Based on existing routine monitoring networks (e.g. MDN, EMEP) and the published literature, global observations including surface Hg concentrations and deposition are collected for model evaluation. Compared with previous studies, many more observations over East Asia (especially China) are included in our dataset. Model evaluation shows that the spatial distribution and seasonal cycle of Hg concentrations and deposition can be reproduced reasonably well by GNAQPMS-Hg. Overall, the simulated annual TGM and wet deposition match observations within a factor of two, and within a factor of five for oxidized mercury and dry deposition. This performance is comparable with other state-of-the-art Hg models. Some model deficiencies have also been identified. GNAQPMS-Hg is systematically biased low relative to cruise observations in the Northern Hemisphere, due to poor representation of the air–sea exchange mechanism for Hg. GNAQPMS-Hg overestimates oxidized mercury concentrations in most parts of the world which may partially be caused by excessive oxidation of Hg(0) by relatively high concentrations of OH and O_3 and uncertainties associated with Hg chemical speciation in emission inventories. The model performs significantly better in North America and Europe than in East Asia. This can probably be attributed to the large uncertainties in emission inventories, coarse model resolution and inconsistency between the simulation and observation periods in East Asia. An online nested simulation with higher resolution ($0.33^{\circ} \times 0.33^{\circ}$) over East Asia was conducted to examine the impact of horizontal resolution on model predictions. Relative to the global simulation, the nested simulation can better resolve high spatial variability of Hg concentrations and deposition over East Asia, can better capture features such as higher wet deposition due to orographic and convective precipitation, and land/ocean contrast. Statistically, the RMSE of simulated wet deposition over East Asia is reduced by 24 % in the nested simulation.

To quantify the impacts of Chinese anthropogenic sources on global Hg levels, a model sensitivity simulation was conducted with Chinese anthropogenic emissions

GMDD
7, 6949–6996, 2014

shut off. The results show that these sources contribute 30 and 62 % of surface mercury concentrations and deposition over China. Outside of China, the largest percentage contributions of 11 and 15.2 % are found in the Korean Peninsula, following by Southeast Asia (10.4 and 8.2 %), Mongolia (6.1 and 8.6 %), and Japan (5.7 and 5.9 %). For regions far away from China, the percentage contributions are relatively small (e.g. 4.2 and 4.8 % over North America; 3.5 and 3.0 % over Europe).

To perfect the model, future improvements will be focused on the following aspects: (1) employing dynamic parameterizations for bidirectional air–surface (sea and land) exchange of Hg (Selin et al., 2008; Bash, 2010; Strode et al., 2007) to better reflect natural emissions (including reemission), (2) including halogen chemistry to characterize MDEs in the Polar regions (Holmes et al., 2010), and (3) reducing uncertainties in the anthropogenic Hg emission inventory, especially the Hg speciation profile. Finally, establishment of routine Hg monitoring networks would be also very helpful for enhancing and improving modeling studies in East Asia.

The Supplement related to this article is available online at doi:10.5194/gmdd-7-6949-2014-supplement.

Acknowledgements. This work is funded by the National Natural Science Foundation of China (no. 41405119), the National Basic Research Program of China (2010CB951800) and the CAS Strategic Priority Research Program (XDB05030200 and XDB05030101). We thank the GEOS-Chem Hg modeling group for sharing observational data of Hg.

References

Ariya, P. A., Khalizov, A., and Gidas, A.: Reactions of gaseous mercury with atomic and molecular halogens: kinetics, product studies, and atmospheric implications, J. Phys. Chem. A, 106, 7310–7320, doi:10.1021/jp020719o, 2002.

GMDD
7, 6949–6996, 2014

Bash, J. O.: Description and initial simulation of a dynamic bidirectional air–surface exchange model for mercury in Community Multiscale Air Quality (CMAQ) model, J. Geophys. Res.-Atmos., 115, D06305, doi:10.1029/2009jd012834, 2010.

Bergan, T. and Rodhe, H.: Oxidation of elemental mercury in the atmosphere: constraints imposed by global scale modelling, J. Atmos. Chem., 40, 191–212, doi:10.1023/a:1011929927896, 2001.

Bullock, O. R. and Brehme, K. A.: Atmospheric mercury simulation using the CMAQ model: formulation description and analysis of wet deposition results, Atmos. Environ., 36, 2135–2146, doi:10.1016/s1352-2310(02)00220-0, 2002.

Bullock Jr., O. R., Atkinson, D., Braverman, T., Civerolo, K., Dastoor, A., Davignon, D., Ku, J.-Y., Lohman, K., Myers, T. C., Park, R. J., Seigneur, C., Selin, N. E., Sistla, G., and Vijayaraghavan, K.: The North American Mercury Model Intercomparison Study (NAMMIS): study description and model-to-model comparisons, J. Geophys. Res.-Atmos., 113, D17310, doi:10.1029/2008jd009803, 2008.

Chang, J. S., Brost, R. A., Isaksen, I. S. A., Madronich, S., Middleton, P., Stockwell, W. R., and Walcek, C. J.: A three-dimensional Eulerian acid deposition model: physical concepts and formulation, J. Geophys. Res.-Atmos., 92, 14681–14700, doi:10.1029/JD092iD12p14681, 1987.

Christensen, J. H., Brandt, J., Frohn, L. M., and Skov, H.: Modelling of Mercury in the Arctic with the Danish Eulerian Hemispheric Model, Atmos. Chem. Phys., 4, 2251–2257, doi:10.5194/acp-4-2251-2004, 2004.

Clever, H. L., Johnson, S. A., and Derrick, M. E.: The solubility of mercury and some sparingly soluble mercury salts in water and aqueous-electrolyte solutions, J. Phys. Chem. Ref. Data, 14, 631–681, 1985.

Corbitt, E. S., Jacob, D. J., Holmes, C. D., Streets, D. G., and Sunderland, E. M.: Global source–receptor relationships for mercury deposition under present-day and 2050 emissions scenarios, Environ. Sci. Technol., 45, 10477–10484, doi:10.1021/es202496y, 2011.

Dastoor, A. and Davignon, D.: Global mercury modelling at Environment Canada, in: Mercury Fate and Transport in the Global Atmosphere, edited by: Mason, R. and Pirrone, N., Springer, New York, USA, 519–532, 2009.

ENVIRON: User's Guide for Comprehensive Air Quality Model with Extensions Version 5.40, ENVIRON International Corporation, Novato, California, 2011.

GMDD

7, 6949–6996, 2014

Frank, D. G.: Mineral Resource Data System (MRDS) Data in Arc-View Shape File Format, for Spatial Data Delivery Project, U.S. Geol. Surv., Spokane, Wash., 1999.
Friedli, H. R., Radke, L. F., Prescott, R., Li, P., Woo, J. H., and Carmichael, G. R.: Mercury in the atmosphere around Japan, Korea, and China as observed during the 2001 ACE-Asia field campaign: measurements, distributions, sources, and implications, J. Geophys. Res.-Atmos., 109, D19s25, doi:10.1029/2003jd004244, 2004.
Friedli, H. R., Arellano, A. F., Cinnirella, S., and Pirrone, N.: Initial estimates of mercury emissions to the atmosphere from global biomass burning, Environ. Sci. Technol., 43, 3507–3513, doi:10.1021/es802703g, 2009.
Fu, X., Feng, X., Sommar, J., and Wang, S.: A review of studies on atmospheric mercury in China, Sci. Total Environ., 421, 73–81, doi:10.1016/j.scitotenv.2011.09.089, 2012.
Ge, B., Wang, Z., Xu, X., Wu, J., Yu, X., and Li, J.: Wet deposition of acidifying substances in different regions of China and the rest of East Asia: modeling with updated NAQPMS, Environ. Pollut., 187, 10–21, doi:10.1016/j.envpol.2013.12.014, 2014.
Granier, C., Lamarque, J. F., Mieville, A., Muller, J. F., and Olivier, J.: POET, a Database of Surface Emissions of Ozone Precursors, tech. report, available at: http://www.aero.jussieu.fr/projet/ACCENT/POET.php (last access: 10 June 2013), 2005.
Guenther, A., Karl, T., Harley, P., Wiedinmyer, C., Palmer, P. I., and Geron, C.: Estimates of global terrestrial isoprene emissions using MEGAN (Model of Emissions of Gases and Aerosols from Nature), Atmos. Chem. Phys., 6, 3181–3210, doi:10.5194/acp-6-3181-2006, 2006.
Hall, B.: The gas phase oxidation of elemental mercury by ozone, Water Air Soil Poll., 80, 301–315, doi:10.1007/bf01189680, 1995.
Hall, B. and Bloom, N.: Report to EPRI, Electric Power Research Institute, Palo Alto, CA, USA, 1993.
Harada, M.: Minamata Disease – methylmercury poisoning in Japan caused by environmental pollution, Crit. Rev. Toxicol., 25, 1–24, doi:10.3109/10408449509089885, 1995.
Holmes, C. D., Jacob, D. J., Corbitt, E. S., Mao, J., Yang, X., Talbot, R., and Slemr, F.: Global atmospheric model for mercury including oxidation by bromine atoms, Atmos. Chem. Phys., 10, 12037–12057, doi:10.5194/acp-10-12037-2010, 2010.
Horowitz, L. W., Walters, S., Mauzerall, D. L., Emmons, L. K., Rasch, P. J., Granier, C., Tie, X. X., Lamarque, J. F., Schultz, M. G., Tyndall, G. S., Orlando, J. J., and Brasseur, G. P.: A global

GMDD
7, 6949–6996, 2014

simulation of tropospheric ozone and related tracers: description and evaluation of MOZART, version 2, J. Geophys. Res.-Atmos., 108, 4784, doi:10.1029/2002jd002853, 2003.
Jaffe, D. and Strode, S.: Sources, fate and transport of atmospheric mercury from Asia, Environ. Chem., 5, 121–126, doi:10.1071/en08010, 2008.
Jaffe, D., Prestbo, E., Swartzendruber, P., Weiss-Penzias, P., Kato, S., Takami, A., Hatakeyama, S., and Kajii, Y.: Export of atmospheric mercury from Asia, Atmos. Environ., 39, 3029–3038, doi:10.1016/j.atmosenv.2005.01.030, 2005.
Jiang, G., Shi, J., and Feng, X.: Mercury pollution in China: an overview of the past and current sources of the toxic metal, Environ. Sci. Technol., 40, 3673–3678, 2006.
Jung, G., Hedgecock, I. M., and Pirrone, N.: ECHMERIT V1.0 – a new global fully coupled mercury-chemistry and transport model, Geosci. Model Dev., 2, 175–195, doi:10.5194/gmd-2-175-2009, 2009.
Keeler, G. J., Pirrone, N., Bullock, R., and Sillman, S.: The need for a coordinated global Hg monitoring network for global and regional models validation, in: Mercury Fate and Transport in the Global Atmosphere, edited by: Mason, R. and Pirrone, N., Springer, New York, USA, 391–424, 2009.
Lamarque, J.-F., Bond, T. C., Eyring, V., Granier, C., Heil, A., Klimont, Z., Lee, D., Liousse, C., Mieville, A., Owen, B., Schultz, M. G., Shindell, D., Smith, S. J., Stehfest, E., Van Aardenne, J., Cooper, O. R., Kainuma, M., Mahowald, N., McConnell, J. R., Naik, V., Riahi, K., and van Vuuren, D. P.: Historical (1850–2000) gridded anthropogenic and biomass burning emissions of reactive gases and aerosols: methodology and application, Atmos. Chem. Phys., 10, 7017–7039, doi:10.5194/acp-10-7017-2010, 2010.
Lamborg, C. H., Fitzgerald, W. F., O'Donnell, J., and Torgersen, T.: A non-steady-state compartmental model of global-scale mercury biogeochemistry with interhemispheric atmospheric gradients, Geochim. Cosmochim. Ac., 66, 1105–1118, doi:10.1016/s0016-7037(01)00841-9, 2002.
Lawrence, M. G., Jöckel, P., and von Kuhlmann, R.: What does the global mean OH concentration tell us?, Atmos. Chem. Phys., 1, 37–49, doi:10.5194/acp-1-37-2001, 2001.
Lei, H., Liang, X.-Z., Wuebbles, D. J., and Tao, Z.: Model analyses of atmospheric mercury: present air quality and effects of transpacific transport on the United States, Atmos. Chem. Phys., 13, 10807–10825, doi:10.5194/acp-13-10807-2013, 2013.

GMDD
7, 6949–6996, 2014

Li, J., Wang, Z., Akimoto, H., Gao, C., Pochanart, P., and Wang, X.: Modeling study of ozone seasonal cycle in lower troposphere over east Asia, J. Geophys. Res.-Atmos., 112, D22s25, doi:10.1029/2006jd008209, 2007.

Li, J., Wang, Z., Wang, X., Yamaji, K., Takigawa, M., Kanaya, Y., Pochanart, P., Liu, Y., Irie, H., Hu, B., Tanimoto, H., and Akimoto, H.: Impacts of aerosols on summertime tropospheric photolysis frequencies and photochemistry over Central Eastern China, Atmos. Environ., 45, 1817–1829, doi:10.1016/j.atmosenv.2011.01.016, 2011.

Li, J., Wang, Z., Zhuang, G., Luo, G., Sun, Y., and Wang, Q.: Mixing of Asian mineral dust with anthropogenic pollutants over East Asia: a model case study of a super-duststorm in March 2010, Atmos. Chem. Phys., 12, 7591–7607, doi:10.5194/acp-12-7591-2012, 2012.

Lin, C. J. and Pehkonen, S. O.: Aqueous free radical chemistry of mercury in the presence of iron oxides and ambient aerosol, Atmos. Environ., 31, 4125–4137, doi:10.1016/S1352-2310(97)00269-0, 1997.

Lin, C. J. and Pehkonen, S. O.: Oxidation of elemental mercury by aqueous chlorine (HOCl/OCl$^-$): implications for tropospheric mercury chemistry, J. Geophys. Res.-Atmos., 103, 28093–28102, doi:10.1029/98jd02304, 1998.

Lin, C. J. and Pehkonen, S. O.: The chemistry of atmospheric mercury: a review, Atmos. Environ., 33, 2067–2079, doi:10.1016/s1352-2310(98)00387-2, 1999.

Lin, C. J., Pongprueks, P., Ho, T. C., and Jang, C.: Development of mercury modeling schemes within CMAQ framework: science and model implementation issues, in: Proceedings of the 2004 CMAS Models-3 Conference, Research Triangle Park, NC, 18–20 October, CD-ROM, 2004.

Lin, C. J., Pongprueksa, P., Lindberg, S. E., Pehkonen, S. O., Byun, D., and Jang, C.: Scientific uncertainties in atmospheric mercury models I: Model science evaluation, Atmos. Environ., 40, 2911–2928, doi:10.1016/j.atmosenv.2006.01.009, 2006.

Lindberg, S., Bullock, R., Ebinghaus, R., Engstrom, D., Feng, X., Fitzgerald, W., Pirrone, N., Prestbo, E., and Seigneur, C.: A synthesis of progress and uncertainties in attributing the sources of mercury in deposition, Ambio, 36, 19–32, 2007.

Lindqvist, O. and Rodhe, H.: Atmospheric mercury – a review, Tellus B, 37, 136–159, 1985.

Mason, R.: Mercury emissions from natural processes and their importance in the global mercury cycle, in: Mercury Fate and Transport in the Global Atmosphere, edited by: Mason, R. and Pirrone, N., Springer, New York, USA, 173–191, 2009.

GMDD

7, 6949–6996, 2014

Munthe, J.: The aqueous oxidation of elemental mercury by ozone, Atmos. Environ., 26, 1461–1468, doi:10.1016/0960-1686(92)90131-4, 1992.
Pacyna, E. G., Pacyna, J. M., Steenhuisen, F., and Wilson, S.: Global anthropogenic mercury emission inventory for 2000, Atmos. Environ., 40, 4048–4063, doi:10.1016/j.atmosenv.2006.03.041, 2006.
Pan, L., Chai, T., Carmichael, G. R., Tang, Y., Streets, D., Woo, J.-H., Friedli, H. R., and Radke, L. F.: Top-down estimate of mercury emissions in China using four-dimensional variational data assimilation, Atmos. Environ., 41, 2804–2819, doi:10.1016/j.atmosenv.2006.11.048, 2007.
Pan, L., Carmichael, G. R., Adhikary, B., Tang, Y., Streets, D., Woo, J.-H., Friedli, H. R., and Radke, L. F.: A regional analysis of the fate and transport of mercury in East Asia and an assessment of major uncertainties, Atmos. Environ., 42, 1144–1159, doi:10.1016/j.atmosenv.2007.10.045, 2008.
Pehkonen, S. O. and Lin, C. J.: Aqueous photochemistry of mercury with organic acids, JAPCA J. Air Waste Ma., 48, 144–150, doi:10.1080/10473289.1998.10463661, 1998.
Pirrone, N. and Keating, T.: Hemispheric Transport of Air Pollution 2010 Part B: Mercury, United Nations Publication, New York and Geneva, 210 pp., 2010.
Pirrone, N., Cinnirella, S., Feng, X., Finkelman, R. B., Friedli, H. R., Leaner, J., Mason, R., Mukherjee, A. B., Stracher, G. B., Streets, D. G., and Telmer, K.: Global mercury emissions to the atmosphere from anthropogenic and natural sources, Atmos. Chem. Phys., 10, 5951–5964, doi:10.5194/acp-10-5951-2010, 2010.
Price, C., Penner, J., and Prather, M.: NO_x from lightning: 1. Global distribution based on lightning physics, J. Geophys. Res.-Atmos., 102, 5929–5941, doi:10.1029/96jd03504, 1997.
Ryaboshapko, A., Bullock, O. R., Jr., Christensen, J., Cohen, M., Dastoor, A., Ilyin, I., Petersen, G., Syrakov, D., Travnikov, O., Artz, R. S., Davignon, D., Draxler, R. R., Munthe, J., and Pacyna, J.: Intercomparison study of atmospheric mercury models: 2. Modelling results vs. long-term observations and comparison of country deposition budgets, Sci. Total Environ., 377, 319–333, doi:10.1016/j.scitotenv.2007.01.071, 2007.
Sanemasa, I.: The solubility of elemental mercury vapor in water, B. Chem. Soc. Jpn., 48, 1795–1798, 1975.
Schroeder, W. H. and Munthe, J.: Atmospheric mercury – an overview, Atmos. Environ., 32, 809–822, doi:10.1016/s1352-2310(97)00293-8, 1998.

GMDD
7, 6949–6996, 2014

Schroeder, W. H., Anlauf, K. G., Barrie, L. A., Lu, J. Y., Steffen, A., Schneeberger, D. R., and Berg, T.: Arctic springtime depletion of mercury, Nature, 394, 331–332, doi:10.1038/28530, 1998.

Seigneur, C., Abeck, H., Chia, G., Reinhard, M., Bloom, N. S., Prestbo, E., and Saxena, P.: Mercury adsorption to elemental carbon (soot) particles and atmospheric particulate matter, Atmos. Environ., 32, 2649–2657, doi:10.1016/S1352-2310(97)00415-9, 1998.

Seigneur, C., Karamchandani, P., Lohman, K., Vijayaraghavan, K., and Shia, R. L.: Multiscale modeling of the atmospheric fate and transport of mercury, J. Geophys. Res.-Atmos., 106, 27795–27809, doi:10.1029/2000jd000273, 2001.

Seigneur, C., Vijayaraghavan, K., Lohman, K., Karamchandani, P., and Scott, C.: Global source attribution for mercury deposition in the United States, Environ. Sci. Technol., 38, 555–569, doi:10.1021/es034109t, 2004.

Selin, N. E.: Global biogeochemical cycling of mercury: a review, Annu. Rev. Env. Resour., 34, 43–63, doi:10.1146/annurev.environ.051308.084314, 2009.

Selin, N. E., Jacob, D. J., Park, R. J., Yantosca, R. M., Strode, S., Jaegle, L., and Jaffe, D.: Chemical cycling and deposition of atmospheric mercury: global constraints from observations, J. Geophys. Res.-Atmos., 112, D02308, doi:10.1029/2006jd007450, 2007.

Selin, N. E., Jacob, D. J., Yantosca, R. M., Strode, S., Jaegle, L., and Sunderland, E. M.: Global 3-D land–ocean–atmosphere model for mercury: present-day versus preindustrial cycles and anthropogenic enrichment factors for deposition, Global Biogeochem. Cy., 22, GB3099, doi:10.1029/2008gb003282, 2008.

Sillen, L. G., Martell, A. E., and Bjerrum, J.: Stability constants of metal-ion complexes, Chemical Society, London, 754 pp., 1964.

Soerensen, A. L., Skov, H., Jacob, D. J., Soerensen, B. T., and Johnson, M. S.: Global concentrations of gaseous elemental mercury and reactive gaseous mercury in the marine boundary layer, Environ. Sci. Technol., 44, 7425–7430, doi:10.1021/es903839n, 2010a.

Soerensen, A. L., Sunderland, E. M., Holmes, C. D., Jacob, D. J., Yantosca, R. M., Skov, H., Christensen, J. H., Strode, S. A., and Mason, R. P.: An improved global model for air–sea exchange of mercury: high concentrations over the North Atlantic, Environ. Sci. Technol., 44, 8574–8580, doi:10.1021/es102032g, 2010b.

Sommar, J., Gardfeldt, K., Stromberg, D., and Feng, X. B.: A kinetic study of the gas-phase reaction between the hydroxyl radical and atomic mercury, Atmos. Environ., 35, 3049–3054, doi:10.1016/s1352-2310(01)00108-x, 2001.

GMDD
7, 6949–6996, 2014

Sprovieri, F., Pirrone, N., Ebinghaus, R., Kock, H., and Dommergue, A.: A review of worldwide atmospheric mercury measurements, Atmos. Chem. Phys., 10, 8245–8265, doi:10.5194/acp-10-8245-2010, 2010.

Steffen, A., Schroeder, W., Macdonald, R., Poissant, L., and Konoplev, A.: Mercury in the Arctic atmosphere: an analysis of eight years of measurements of GEM at Alert (Canada) and a comparison with observations at Amderma (Russia) and Kuujjuarapik (Canada), Sci. Total Environ., 342, 185–198, doi:10.1016/j.scitotenv.2004.12.048, 2005.

Strode, S. A., Jaegle, L., Selin, N. E., Jacob, D. J., Park, R. J., Yantosca, R. M., Mason, R. P., and Slemr, F.: Air–sea exchange in the global mercury cycle, Global Biogeochem. Cy., 21, GB1017, doi:10.1029/2006gb002766, 2007.

Strode, S. A., Jaegle, L., Jaffe, D. A., Swartzendruber, P. C., Selin, N. E., Holmes, C., and Yantosca, R. M.: Trans-Pacific transport of mercury, J. Geophys. Res.-Atmos., 113, D15305, doi:10.1029/2007jd009428, 2008.

Tang, X., Wang, Z., Zhu, J., Gbaguidi, A. E., Wu, Q., Li, J., and Zhu, T.: Sensitivity of ozone to precursor emissions in urban Beijing with a Monte Carlo scheme, Atmos. Environ., 44, 3833–3842, doi:10.1016/j.atmosenv.2010.06.026, 2010.

Taylor, K. E.: Summarizing multiple aspects of model performance in a single diagram, J. Geophys. Res.-Atmos., 106, 7183–7192, doi:10.1029/2000jd900719, 2001.

Temme, C., Slemr, F., Ebinghaus, R., and Einax, J. W.: Distribution of mercury over the Atlantic Ocean in 1996 and 1999–2001, Atmos. Environ., 37, 1889–1897, doi:10.1016/s1352-2310(03)00069-4, 2003.

Tokos, J. J. S., Hall, B., Calhoun, J. A., and Prestbo, E. M.: Homogeneous gas-phase reaction of Hg0 with H_2O_2, O_3, CH_3I, and $(CH_3)_2S$: implications for atmospheric Hg cycling, Atmos. Environ., 32, 823–827, doi:10.1016/s1352-2310(97)00171-4, 1998.

Travnikov, O.: Contribution of the intercontinental atmospheric transport to mercury pollution in the Northern Hemisphere, Atmos. Environ., 39, 7541–7548, doi:10.1016/j.atmosenv.2005.07.066, 2005.

Travnikov, O. and Ilyin, I.: The EMEP/MSC-E mercury modeling system, in: Mercury Fate and Transport in the Global Atmosphere, edited by: Mason, R. and Pirrone, N., Springer, New York, USA, 571–587, 2009.

Van Loon, L., Mader, E., and Scott, S. L.: Reduction of the aqueous mercuric ion by sulfite: UV spectrum of $HgSO_3$ and its intramolecular redox reaction, J. Phys. Chem. A, 104, 1621–1626, doi:10.1021/jp994268s, 2000.

GMDD
7, 6949–6996, 2014

Van Loon, L. L., Mader, E. A., and Scott, S. L.: Sulfite stabilization and reduction of the aqueous mercuric ion: kinetic determination of sequential formation constants, J. Phys. Chem. A, 105, 3190–3195, doi:10.1021/jp003803h, 2001.

Voulgarakis, A., Naik, V., Lamarque, J.-F., Shindell, D. T., Young, P. J., Prather, M. J., Wild, O., Field, R. D., Bergmann, D., Cameron-Smith, P., Cionni, I., Collins, W. J., Dalsøren, S. B., Doherty, R. M., Eyring, V., Faluvegi, G., Folberth, G. A., Horowitz, L. W., Josse, B., MacKenzie, I. A., Nagashima, T., Plummer, D. A., Righi, M., Rumbold, S. T., Stevenson, D. S., Strode, S. A., Sudo, K., Szopa, S., and Zeng, G.: Analysis of present day and future OH and methane lifetime in the ACCMIP simulations, Atmos. Chem. Phys., 13, 2563–2587, doi:10.5194/acp-13-2563-2013, 2013.

Walcek, C. J. and Aleksic, N. M.: A simple but accurate mass conservative, peak-preserving, mixing ratio bounded advection algorithm with Fortran code, Atmos. Environ., 32, 3863–3880, doi:10.1016/s1352-2310(98)00099-5, 1998.

Wang, Q., Fu, Q., Wang, Z., Wang, T., Liu, P., Lu, T., Duan, Y., and Huang, Y.: Application of ensemble numerical model system on the air quality forecast in Shanghai, Environmental Monitoring and Forewarning, 2, 1–6, 2010 (in Chinese).

Wang, Z., Akimoto, H., and Uno, I.: Neutralization of soil aerosol and its impact on the distribution of acid rain over east Asia: observations and model results, J. Geophys. Res.-Atmos., 107, 4389, doi:10.1029/2001jd001040, 2002.

Wang, Z., Xie, F., Wang, X., An, J., and Zhu, J.: Development and application of nested air quality prediction modeling system, Chinese Journal of Atmospheric Science, 30, 778–790, 2006 (in Chinese).

Wang, Z., Wu, Q., Gbaguidi, A., Yan, P., Zhang, W., Wang, W., and Tang, X.: Ensemble air quality multi-model forecast system for Beijing (EMS-Beijing): model description and preliminary application, Journal of Nanjing University of Information Science & Technology (Natural Science Edition), 1, 19–26, 2009 (in Chinese).

Wesely, M. L.: Parameterization of surface resistances to gaseous dry deposition in regional-scale numerical models, Atmos. Environ., 23, 1293–1304, doi:10.1016/0004-6981(89)90153-4, 1989.

Wilson, S. J., Steenhuisen, F., Pacyna, J. M., and Pacyna, E. G.: Mapping the spatial distribution of global anthropogenic mercury atmospheric emission inventories, Atmos. Environ., 40, 4621–4632, doi:10.1016/j.atmosenv.2006.03.042, 2006.

GMDD
7, 6949–6996, 2014

Wu, Q., Wang, Z., Chen, H., Zhou, W., and Wenig, M.: An evaluation of air quality modeling over the Pearl River Delta during November 2006, Meteorol. Atmos. Phys., 116, 113–132, doi:10.1007/s00703-011-0179-z, 2012.

Yan, X., Ohara, T., and Akimoto, H.: Statistical modeling of global soil NO_x emissions, Global Biogeochem. Cy., 19, GB3019, doi:10.1029/2004GB002276, 2005.

Zhang, Y., Jaeglé, L., van Donkelaar, A., Martin, R. V., Holmes, C. D., Amos, H. M., Wang, Q., Talbot, R., Artz, R., Brooks, S., Luke, W., Holsen, T. M., Felton, D., Miller, E. K., Perry, K. D., Schmeltz, D., Steffen, A., Tordon, R., Weiss-Penzias, P., and Zsolway, R.: Nested-grid simulation of mercury over North America, Atmos. Chem. Phys., 12, 6095–6111, doi:10.5194/acp-12-6095-2012, 2012.

Zaveri, R. and Peters, L.: A new lumped structure photochemical mechanism for large-scale applications, J. Geophys. Res.-Atmos., 104, 30387–30415, 1999.

GMDD

7, 6949–6996, 2014

Table 1. Reactions and rate constants used in the GNAQPMS-Hg model.

NO.	Reaction	Rates (k or K)	References
Gas-phase reactions			
RG1	$Hg(0)(g) + O_3(g) \rightarrow Hg(II)(g)$	$3 \times 10^{-20}\ cm^3\ molec^{-1}\ s^{-1}$	Hall (1995)
RG2	$Hg(0)(g) + HCl(g) \rightarrow HgCl_2(g)$	$1 \times 10^{-19}\ cm^3\ molec^{-1}\ s^{-1}$	Hall and Bloom (1993)
RG3	$Hg(0)(g) + H_2O_2(g) \rightarrow Hg(OH)_2(g)$	$8.5 \times 10^{-19}\ cm^3\ molec^{-1}\ s^{-1}$	Tokos et al. (1998)
RG4	$Hg(0)(g) + Cl_2(g) \rightarrow HgCl_2(g)$	$2.6 \times 10^{-18}\ cm^3\ molec^{-1}\ s^{-1}$	Ariya et al. (2002)
RG5	$Hg(0)(g) + OH(g) \rightarrow Hg(OH)_2(g)$	$8 \times 10^{-14}\ cm^3\ molec^{-1}\ s^{-1}$	Sommar et al. (2001)
Gas-liquid equilibria			
GL1	$Hg(0)(g) \leftrightarrow Hg(0)(aq)$	$0.11\ M\ atm^{-1}$	Sanemasa (1975)
GL2	$HgCl_2(g) \leftrightarrow HgCl_2(aq)$	$1.4 \times 10^{6}\ M\ atm^{-1}$	Lindqvist and Rodhe (1985)
GL3	$Hg(OH)_2(g) \leftrightarrow Hg(OH)_2(aq)$	$1.2 \times 10^{4}\ M\ atm^{-1}$	Lindqvist and Rodhe (1985)
Aqueous-phase equilibria			
AE1	$HgCl_2(aq) \leftrightarrow Hg^{2+} + 2Cl^-$	$1 \times 10^{-14}\ M^2$	Sillen et al. (1964)
AE2	$Hg(OH)_2(aq) \leftrightarrow Hg^{2+} + 2OH^-$	$1 \times 10^{-22}\ M^2$	Sillen et al. (1964)
AE3	$Hg^{2+} + SO_3^{2-} \leftrightarrow HgSO_3$	$2.1 \times 10^{13}\ M^{-1}$	Van Loon et al. (2001)
AE4	$HgSO_3 + SO_3^{2-} \leftrightarrow Hg(SO_3^{2-})$	$1 \times 10^{10}\ M^{-1}$	Van Loon et al. (2001)
Aqueous-phase reaction			
RA1	$Hg(0)(aq) + O_3(aq) \rightarrow Hg^{2+}$	$4.7 \times 10^{7}\ M^{-1}\ s^{-1}$	Munthe (1992)
RA2	$Hg(0)(aq) + OH(aq) \rightarrow Hg^{2+}$	$2 \times 10^{9}\ M^{-1}\ s^{-1}$	Lin and Pehkonen (1997)
RA3	$HgSO_3(aq) \rightarrow Hg(0)(aq)$	$0.0106\ s^{-1}$	Van Loon et al. (2000)
RA4	$Hg(II)(aq) + HO_2(aq) \rightarrow Hg(0)(aq)$	$1.7 \times 10^{4}\ M^{-1}\ s^{-1}$	Pehkonen and Lin (1998)
RA5	$Hg(0)(aq) + HOCl(aq) \rightarrow Hg^{2+}$	$2.09 \times 10^{6}\ M^{-1}\ s^{-1}$	Lin and Pehkonen (1998)
RA6	$Hg(0)(aq) + OCl^- \rightarrow Hg^{2+}$	$1.99 \times 10^{6}\ M^{-1}\ s^{-1}$	Lin and Pehkonen (1998)
Adsorption of Hg(II) on PM in the aqueous-phase			
AD1	$Hg(II)(aq) \leftrightarrow Hg(II)(p)$	$34\ L\ g^{-1}$	Seigneur et al. (1998)

GMDD
7, 6949–6996, 2014

Table 2. Global budgets of TGM in the literature (unit: Mg yr^{-1}).

	Bergan et al. (1999)	Shia et al. (1999)	Lamborg et al. (2002)	Mason et al. (2002)	Seigneur et al. (2004)	Selin et al. (2007)	Selin et al. (2008)	This work
Total Sources	6050	6100	4400	6600	6411	7000	11 200	10 163
anthropogenic	2150	2100	2600	2400	2143	2200	3400	2488
land	2500	2000	1000	1600	2290	2000	2800	2675
ocean	1400	2000	800	2600	1978	2800	5000	5000
Total Sinks	6050	6100	4200	6600	6411	7000	11 200	10 163
Wet deposition		2800		3920		2100		2283
Dry deposition		3300		2680		4700		7880
TGM Burden	6050	10 400	5220	5000	7690	5360	5600	8619
TGM lifetime (yr)	1	1.7	1.3	0.76	1.2	0.79	0.5	0.85

GMDD
7, 6949–6996, 2014

Table 3. Statistical summary of comparisons of the model results with observations[a].

Parameter	Region	*R*	NMB	RMSE	SVR[b]
TGM	East Asia Nested	0.51	−39 %	3.87	2.56
	East Asia	0.54	−32 %	3.61	2.56
	North America	0.69	18 %	0.58	0.48
	Europe	0.57	−8 %	0.17	0.35
	Global	0.70	−18 %	2.22	–
Oxidized mercury	East Asia Nested	0.45	−12 %	242	3.66
	East Asia	0.31	−10 %	259	3.66
	North America	0.53	148 %	28	1.61
	Europe	0.91	155 %	48	1.00
	Global	0.53	3 %	185	–
Wet deposition	East Asia Nested	0.78	−28 %	45.5	6.69
	East Asia	0.36	−61 %	60.1	6.69
	North America	0.76	−4 %	4.3	1.89
	Europe	0.78	4 %	1.5	1.40
	Global	0.38	−36 %	29.3	–
Dry deposition	East Asia Nested	0.88	−42 %	87.0	–
	East Asia	0.81	−42 %	88.5	–

[a] *R*, NMB, RMSE, SVR represent correlation coefficient, normalized mean bias, root mean square error, spatial variation ratio. Units of TGM, oxidized mercury, wet and dry deposition are $ng\,m^{-3}$, $pg\,m^{-3}$, $\mu g\,m^{-2}\,yr^{-1}$, $\mu g\,m^{-2}\,yr^{-1}$ respectively.
[b] SVR defines as (max – min)/mean observations over all sites.

GMDD
7, 6949–6996, 2014

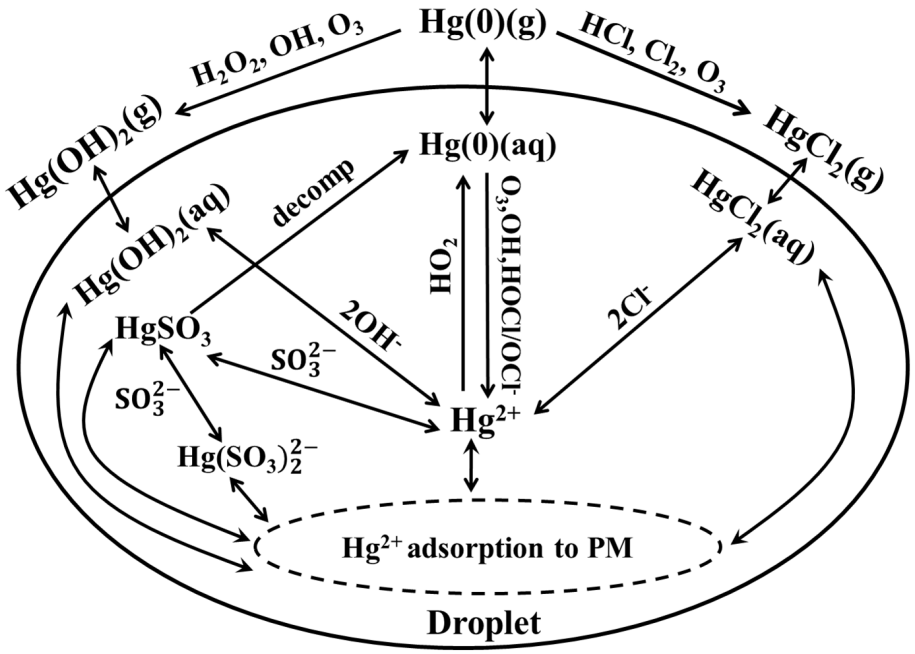

Figure 1. Schematic of different mercury reactions utilized in the GNAQPMS-Hg model.

GMDD
7, 6949–6996, 2014

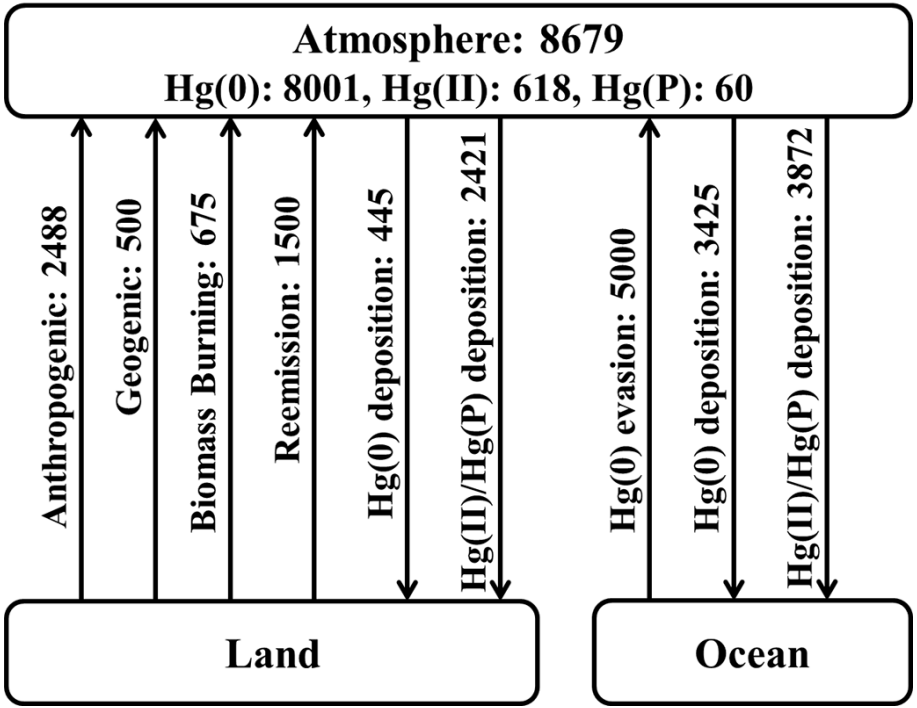

Figure 2. Global atmospheric mercury budget in GNAQPMS-Hg. Units are Mg yr^{-1}.

GMDD
7, 6949–6996, 2014

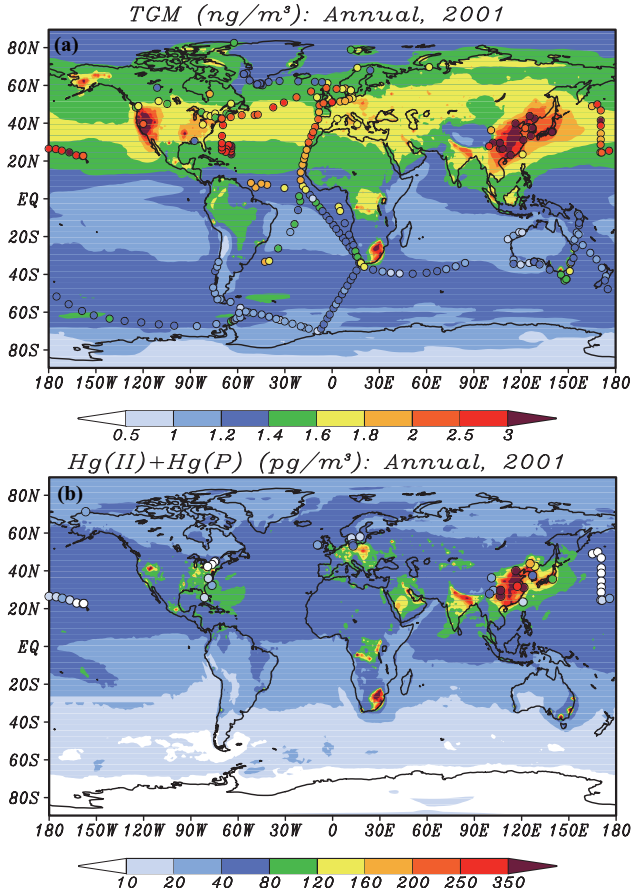

Figure 3. Annual average TGM **(a)** and oxidized mercury (Hg(II)+Hg(P)), **(b)** concentrations in surface air. Model results (background, for year 2001) are compared to observations (circles) from long-term surface sites and short-term ship cruises.

GMDD
7, 6949–6996, 2014

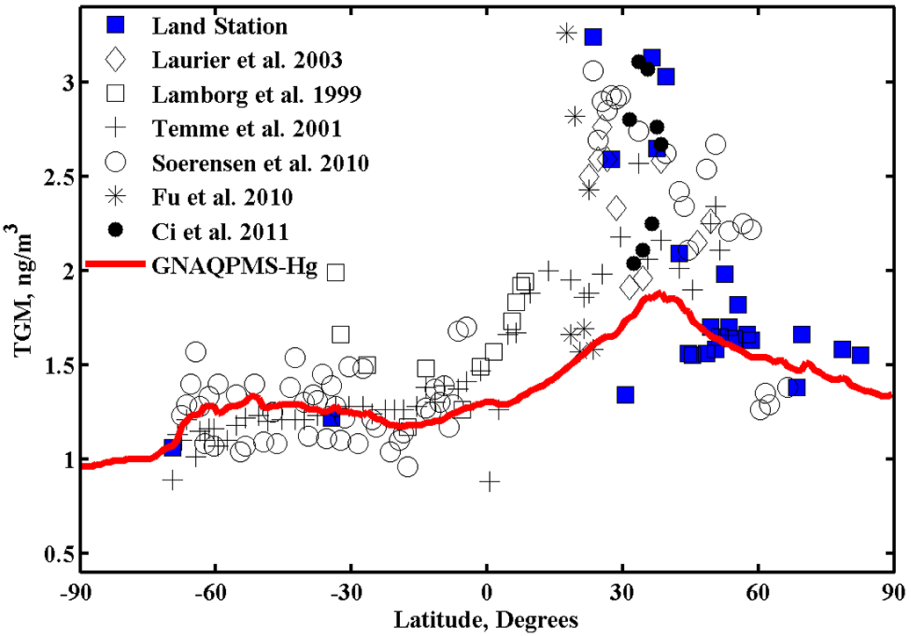

Figure 4. Variation of TGM surface concentrations with latitude. Zonally averaged, annual mean model results (line) are compared to observations (symbols).

GMDD
7, 6949–6996, 2014

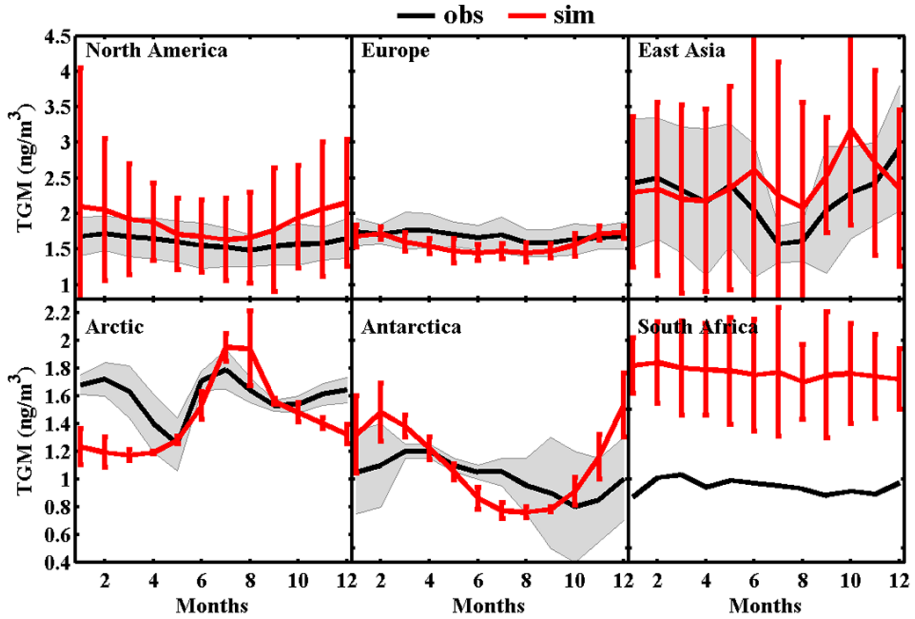

Figure 5. Mean seasonal variation of TGM at North America, Europe, East Asia, Arctic, Antarctica and South Africa sites. Gray shaded areas and red vertical bars show one SD over the sites for observations and for model results.

GMDD
7, 6949–6996, 2014

GNAQPMS-Hg v1.0: a global nested atmospheric mercury transport model

H. S. Chen et al.

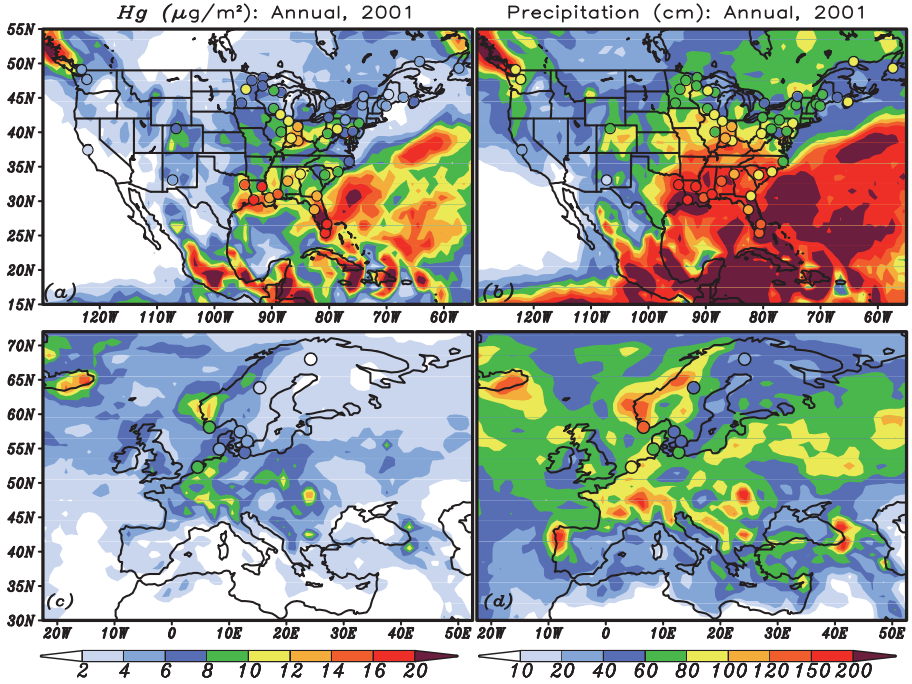

Figure 6. Simulated annual mercury wet deposition and accumulated precipitation over North America **(a, b)** and Europe **(c, d)** in 2001. Overlaid points show observations for the same year from the Mercury Deposition Network (MDN) over North America, and the European Monitoring and Evaluation Programme (EMEP) over Europe.

GMDD
7, 6949–6996, 2014

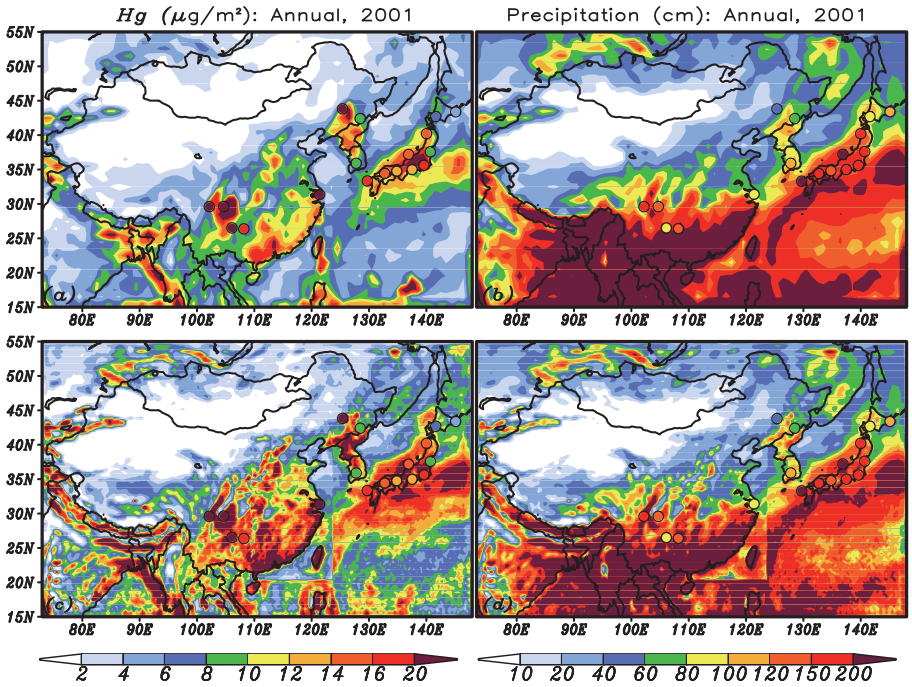

Figure 7. Simulated annual mercury wet deposition and accumulated precipitation over East Asia in the global **(a, b)** and nested **(c, d)** domains in 2001. Overlaid points show observations collected from the literature. Note that observations and simulated results are not in the same year.

GMDD
7, 6949–6996, 2014

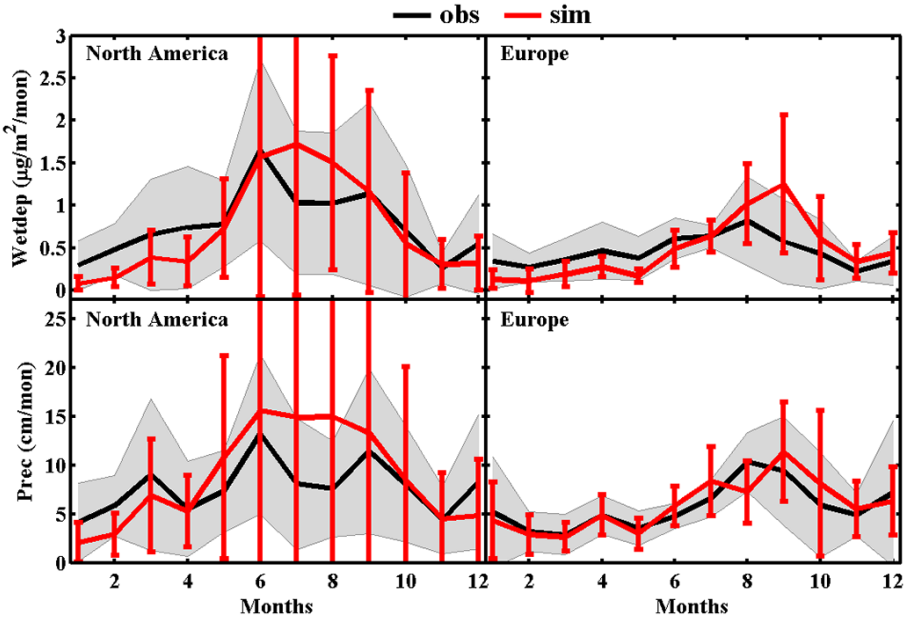

Figure 8. Mean seasonal variation of mercury wet deposition and accumulated precipitation at North America (51 sites averaged) and Europe (8 sites averaged) sites in 2001. Gray shaded areas and red vertical bars show one SD over the sites for observations and for model results.

GMDD
7, 6949–6996, 2014

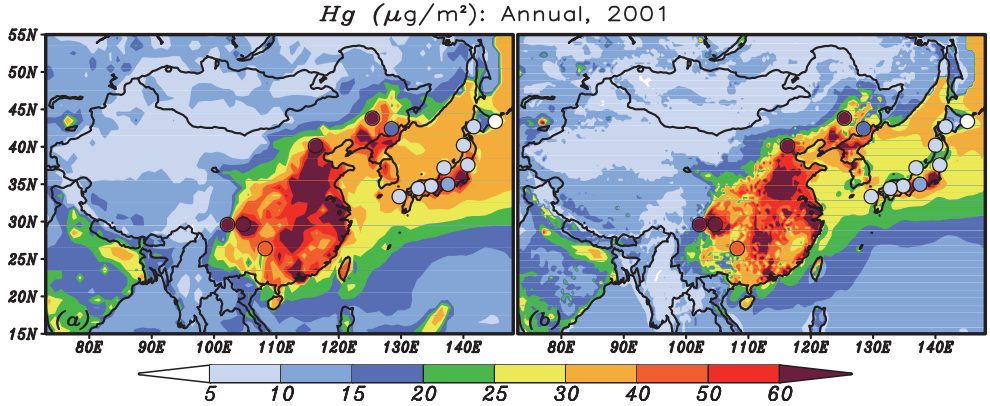

Figure 9. Simulated annual mercury dry deposition over East Asia in the global **(a)** and nested **(b)** domains in 2001. Overlaid points show observations collected from the literature. Note that observations and simulated results are not in the same year.

GMDD
7, 6949–6996, 2014

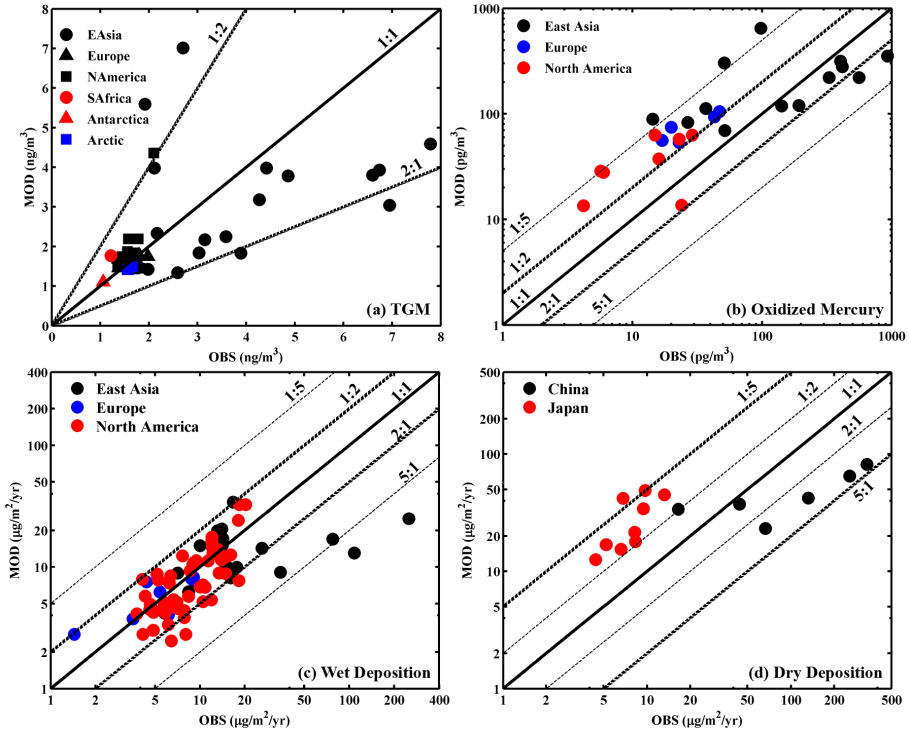

Figure 10. Simulated vs. observed TGM **(a)**, oxidized mercury **(b)**, wet deposition **(c)**, dry deposition **(d)** in different regions. Note that coordinates are different in different panels.

GMDD
7, 6949–6996, 2014

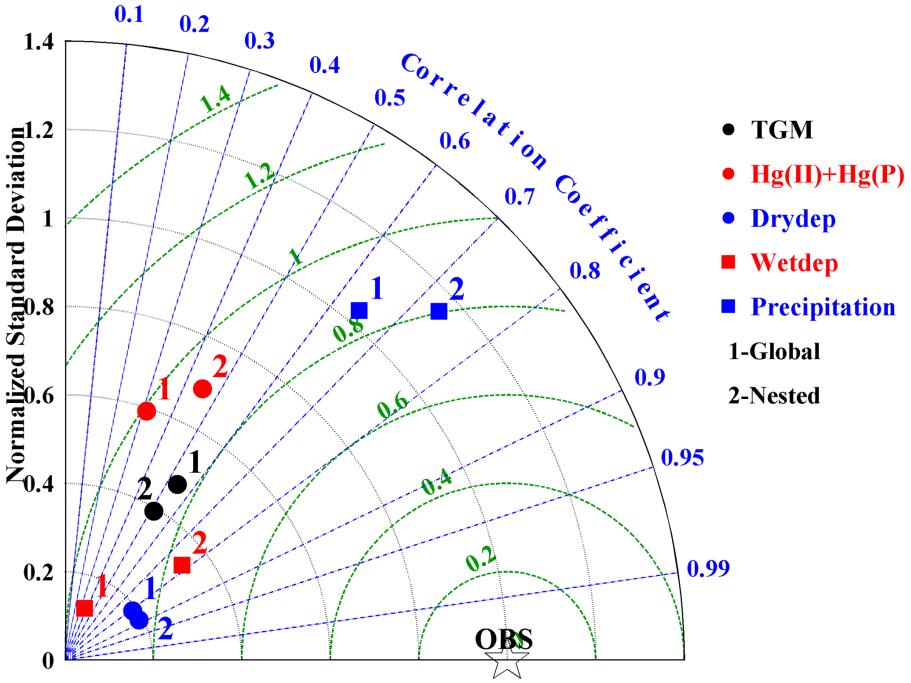

Figure 11. Taylor diagram of simulated annual TGM, Hg(II) + Hg(P), dry deposition, wet deposition and precipitation over East Asia in the global and nested domains (denoted by 1 and 2).

GMDD
7, 6949–6996, 2014

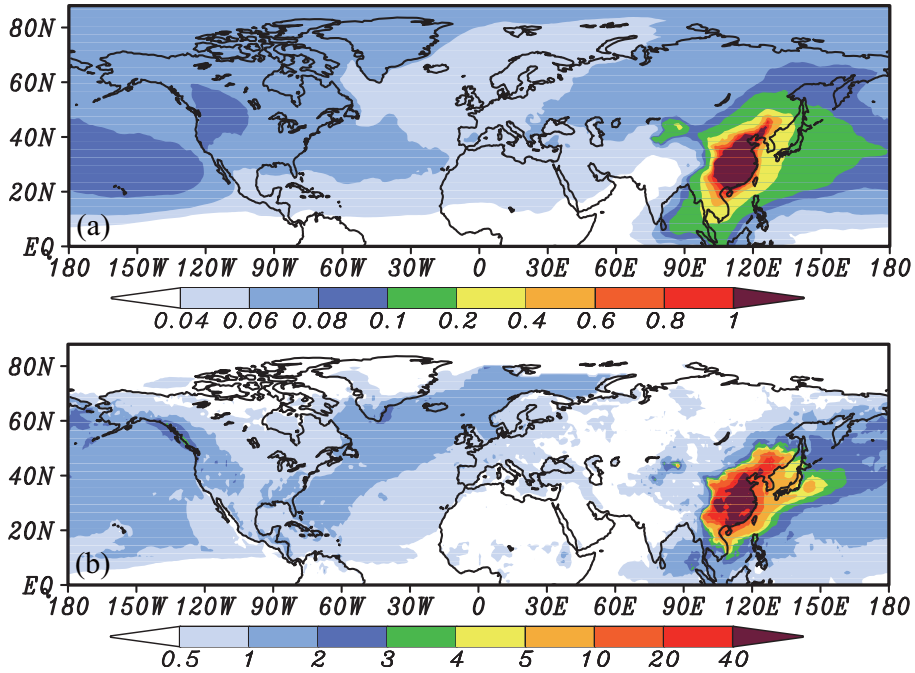

Figure 12. Contributions of Chinese primary anthropogenic sources to **(a)** annual mercury surface concentrations and **(b)** total (wet plus dry) deposition in the Northern Hemisphere. The units for mercury concentrations and deposition are ng m^{-3} and µg m^{-2}, respectively.

GMDD
7, 6949–6996, 2014

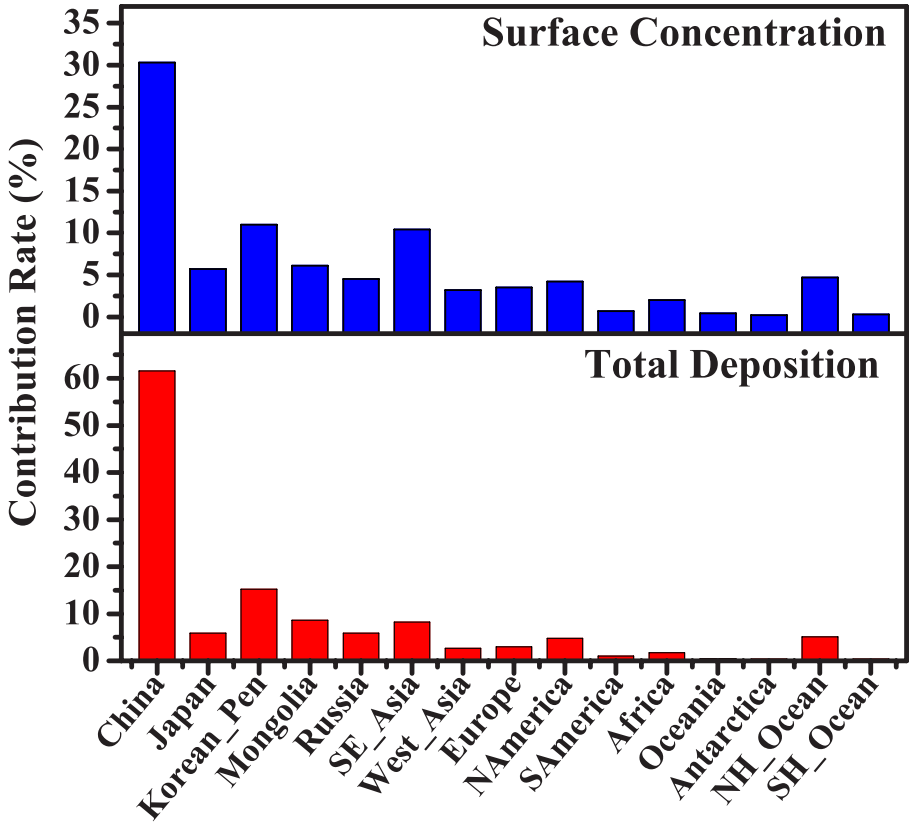

Figure 13. Mean percentage contributions from Chinese primary anthropogenic sources to annual mercury surface concentrations and total (wet plus dry) deposition over different world regions.

GMDD
7, 6949–6996, 2014